The global burden of plant disease tracks crop yields under climate change

Thomas M. Chaloner[1], Sarah J. Gurr[1,2] and Daniel P. Bebber[1*]

[1] Department of Biosciences, University of Exeter, Exeter, EX4 4QD, UK

[2] Department of Biosciences, Utrecht University, Paduallaan 8, Netherlands.

* Correspondence to d.bebber@exeter.ac.uk, tel. +44 1392 725851

Abstract

Global food security is strongly determined by crop production. Climate change will not only affect crop yields directly, but also indirectly via the distributions and impacts of plant pathogens that can cause devastating production losses. However, the likely changes in pathogen pressure in relation to global crop production are poorly understood. Here we show that disease risk for 79 fungal and oomycete crop pathogens will closely track projected yield changes in 12 major crops over the 21st Century. For most crops, yields are likely to increase at high latitudes but disease risk will also grow. In addition, the USA, Europe and China will experience major changes in pathogen assemblages. In contrast, while the tropics will see little or no productivity gains, the disease burden is also likely to decline. The benefits of yield gains will therefore be tempered by the increased burden of crop protection.

Main text

Plant pests and pathogens exert a growing burden on crop production around the world [1,2]. The burden can be measured directly in yield losses or indirectly in the social, environmental and economic costs of control [1]. Like all species, crop pests and pathogens have particular tolerances to, or requirements for, particular environmental conditions [3]. These tolerances define their ecological niche, which determines the geographical regions and periods of the year that allow pests and pathogens to proliferate and attack crops [3]. As climate changes, suitable conditions for pest outbreaks shift in time and space, altering the threats that farmers face and the management regimes required for their control [4]. Modelling the pattern and process of future changes in pest and pathogen burdens is therefore a key component in maintaining future food security [5].

Latitudinal range shifts of pests and pathogens are expected as the planet warms and populations track their preferred temperature zones [4]. Spatial movements in geographical distributions and temporal shifts in phenologies of wild populations are among the clearest signs of anthropogenic global warming [6]. Though distribution data for crop pests and pathogens are noisy and incomplete [5], similar changes have been detected for hundreds a species of pests and pathogens over recent decades [7]. Increasing burdens of insect pests at high latitudes, and decreasing burdens at low latitudes, have been projected using ecological niche models (ENM) [8]. ENMs attempt to reconstruct the environmental tolerances of species from contemporary climates within the observed species range using statistical models [9]. Alternatively, species' responses to microclimate can be directly measured, and these responses incorporated into physiologically-based models of species performance [10]. Such mechanistic models are commonly used to project future crop yields [11], and models have also been developed for some plant diseases [12,13]. However, we know little about how plant disease pressure is likely to change in future, nor how these changes will relate to crop yield responses to climate change. Here, we analyse temperature response functions for host infection for a suite of fungal and oomycete plant pathogens, and model the likely shifts in infection risk globally for the 21st Century. We compare climate-driven changes in infection risk with projected changes in crop yields to reveal how the global burden of plant disease will impact upon crop productivity.

Projected crop yield changes

Yields of both temperate and tropical crops are projected to increase at higher latitudes over the 21st Century (Figs. S1-S4). We compared current (2011-2030 mean) and future (2061-2080 mean) yields projections from three crop models (LPJmL, GEPIC, PEPIC) employing four GCMs (GFDL-ESM2M, HADGEM2-ES, IPSL-CM5A-LR, MIROC5) under the RCP6.0 representative concentration pathway. Carbon dioxide fertilization effects were included but potential irrigation was not. The major commodity crops of maize, wheat, soybean and rice, and are considered in all three crop models. Maize yields are projected to increase at higher latitudes (above approx. 40 °), particularly in North America, in all model combinations, with yield declines at lower latitudes. GEPIC/PEPIC project substantial maize yield declines in Central and Latin America except for Argentina, and across Africa and northern Australia. LPJmL projects no such yield declines. Wheat yields also increase at high latitudes in all three crop models, with smaller increases at low latitudes in LPJmL and

declines in GEPIC/PEPIC. North America and parts of Eurasia show the largest wheat yield increases, while GEPIC projects large declines in yield across the tropics. A similar latitudinal trend is projected for soybean but with little decline in the tropics. Soybean yield increases are projected across Eurasia in all models, and also Argentina and South Africa in GEPIC/PEPIC. The latitudinal gradient is less pronounced for rice, with the MIROC5 climate model suggesting a large increase in yield in the Southern hemisphere. MIROC5 is more likely than other climate models to lead to large yield increases for several crops in the Southern hemisphere.

Eight further temperate and tropical annual crops are considered in LPJmL. Cassava yields increase under all four GCMs within 40 ° of latitude, driven by large increases in India. However, all four GCMS suggest a smaller increase within 10 °N, caused by a yield decline in northern Brazil. Peanut, pea, rapeseed, sugarbeet, and sunflower show increases at all latitudes, with the largest increases at higher latitudes. Millet also show increases at high latitudes, but yield declines at low latitudes. There are no consistent differences among the four GCMs for any of the crops. Results for sugarcane are more variable. Mean yield change projections suggest declines in Brazil and other Latin American countries, and in Southeast Asia, but an increase in the USA and in East Africa. Previous analyses based on the more extreme RCP 8.5 scenario similar yield increases with latitude latitudes, but more severe declines for some crops at low latitudes [14].

Total projected crop production change is difficult to estimate because the spatial distributions of planted areas are impossible to predict, due to the influence of socioeconomic and cultural factors on planting choice. However, if production is calculated from projected yield changes on an estimate of current crop production, increases in production are expected for many crops (Fig. S5). Global wheat, cassava, rapeseed and sunflower production are predicted to increase by all models. LPJmL, and two climate models driving GEPIC/PEPIC, predict increases for rice. All models except HADGEM2-ES predict global soybean production increases (see Methods for analysis of soybean production). None of the crop models unequivocally project declines in production for any crop. In summary, crop models project global production increases driven primarily by yield increases at high latitudes, even without changes in cropping patterns to match shifts in areas likely to be most productive.

Projected pathogen pressure changes

Could these yield increases be offset by increasing pathogen pressure? Infection rates by plant pathogens are strongly determined by abiotic conditions, including temperature [3]. We estimated relative infection rates of 79 fungal and oomycete plant pathogens, for which minimum, optimum and maximum infection temperatures were available in the literature [3] (Fig. 1, Table S1). We chose to model experimentally-derived infection temperature responses rather than the more commonly-measured growth in culture, because *in planta* responses differ substantially from *in vitro* responses [3]. Essentially, the temperature range for infection is narrower, and optimum temperature lower, than for growth in culture. However, for two important pathogens, *Magnaporthe oryzae* (causing rice blast) and *Zymoseptoria tritici* (Septoria tritici blotch of wheat), infection temperatures were not available therefore we used lesion development and growth in culture temperatures, respectively. Optimum infection temperatures varied from 10.5 to 34.67 °C among species (median 22.0, IQR 19.36 - 25.00). As global temperatures rise (Fig. S6), infection risks (and distributions) of these pathogens should shift latitudinally [4].

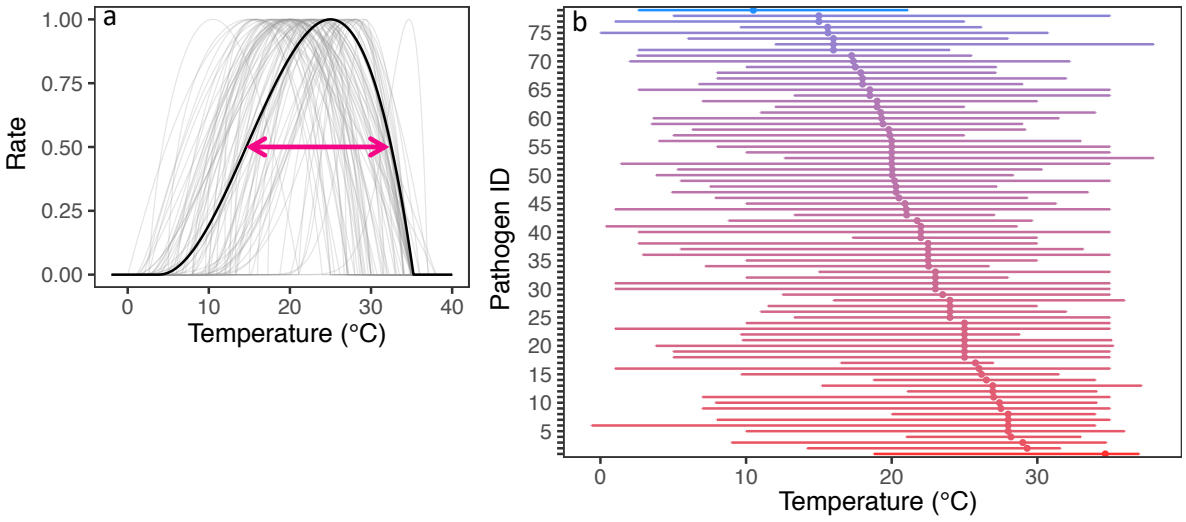

Fig 1. Summary infection cardinal temperature for 79 plant pathogens included in this study. (a) Cardinal temperature geometry determined by estimated T_{min}, T_{opt}, and T_{max}, as well as Equation S1. Pink line refers to temperatures within $T_{range(0.5)}$ of the infection cardinal temperature for an example pathogen. (b) Points refer to T_{opt}, bars refer to T_{range}. Colour refers to T_{opt}. Blue and red refer to cool- and hot-adapted pathogens, respectively. Pathogen ID in Table S1.

Defining pathogen burden as the number of pathogens with high infection risk (relative rate ≥ 0.5) for their hosts in a particular location (Figs. S7, S8), we found that the overall change in burden decreases at low latitudes, and increases at high latitudes, by the end of the 21st Century under RCP 6.0 (Fig. 2a). Europe and China are particularly vulnerable to increasing pathogen burden, while Brazil, sub-Saharan Africa, India and Southeast Asia are likely to have reduced disease burdens. Rapid global dissemination by international trade and transport [15] means that these pathogens are likely to reach all suitable areas that are not yet affected (Fig. S9).

Pathogen burdens are projected to vary through the year, with the largest increases in North America, Europe and China during northern-Hemisphere autumn (Figs. 3, S10). Decreases in pathogen burden are expected at low to mid latitudes in northern-Hemisphere winter, shifting northwards into higher latitudes during summer. For the pathogens we modelled, India is expected to see large declines in infection risk over much of the year, with increases in northern parts of India only in winter. Under increasingly strong greenhouse gas emissions scenarios, the overall latitudinal patterns of pathogen burden and compositional change in both Hemispheres remain the same, but their amplitudes increase (Fig. 4). Burdens decline at low latitudes and increase at high latitudes, while compositional changes peaks at around 10° and 30-40°.

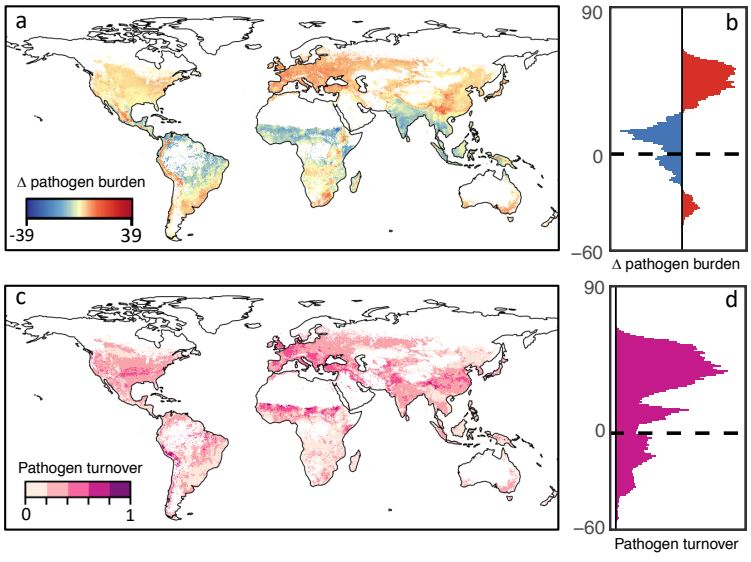

Fig 2. Average change in (a, b) pathogen burden and (c, d) pathogen turnover under RCP 6.0 across all months. Pathogens restricted by host distributions extracted from EarthStat. White grid cells contain no hosts in the EarthStat database, and were excluded from the analysis.

Future changes in pathogen burden closely mirror changes in yield by latitude for the majority of crops (Fig. 5). The majority of rice pathogens in our sample show increased infection risk across all latitudes, with few showing a widespread decline in the tropics. While the infection risk of several maize pathogens is expected to increase at low latitudes, the risk from many others will decline. Maize, millet and sugarcane are expected to undergo yield declines at low latitudes, but these will be accompanied by declines in infection risk from many of their pathogens. Soybean, sunflower and wheat show little yield gain in the tropics, while experiencing reduced infection risk from a number of pathogens. Conversely, both yields and pathogen burden increase strongly with latitude. Cassava pathogen burden generally increases near the equator. Overall, high latitudes will see increasing potential crop yields while simultaneously facing a larger burden of fungal and oomycete pathogens.

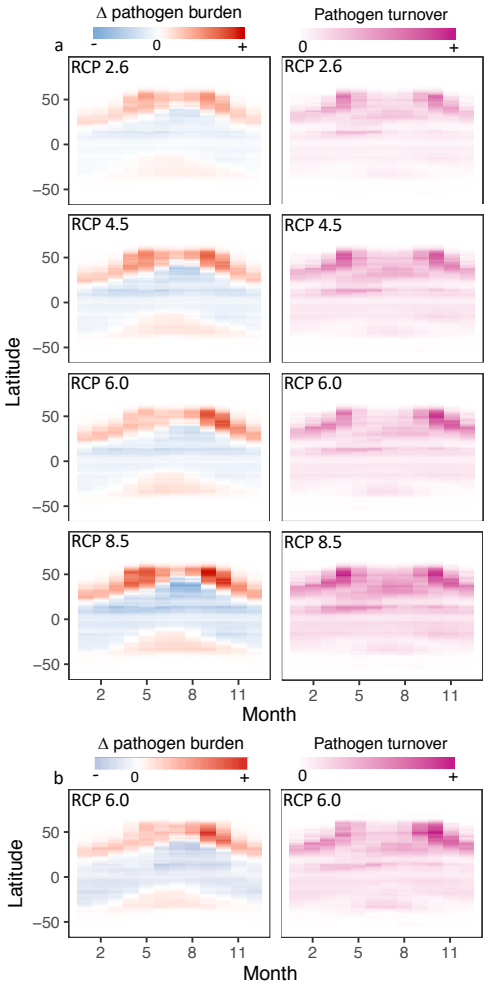

Fig 3. Impact of RCP and pathogen restriction method on change in pathogen burden and turnover. Red and blue indicate increases and decreases in pathogen burden, respectively. Darker pink indicates larger changes in pathogen turnover. Pathogens restricted by estimates

of host distributions extracted from (a) EarthStat and (b) MIRCA2000. Fewer pathogens included in (b) due to fewer host distributions available.

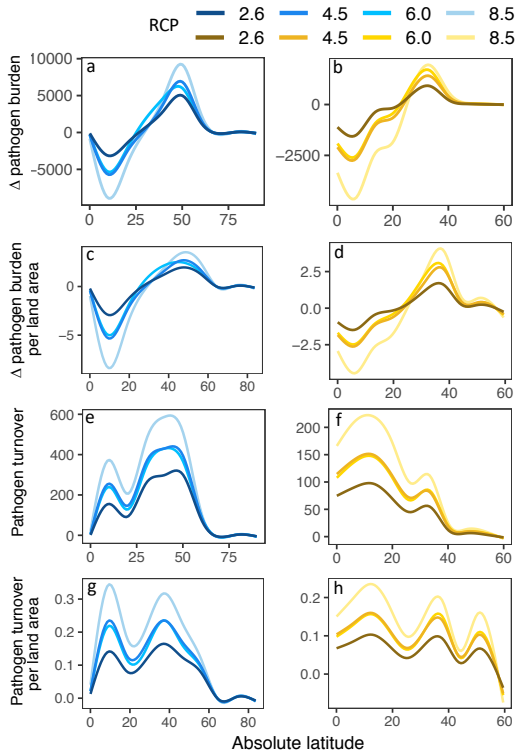

Fig. 4. Impact of RCP on change of pathogen burden and species turnover. (a, c, e, g) Northern hemisphere. (b, d, f, h) Southern Hemisphere.

Changing climate will affect not only the number of pathogens able to infect crops, but also the compositions of pathogen assemblages (Figs. 2cd). Overall, the largest changes in pathogen species composition will occur at high latitudes in the northern Hemisphere, particularly in Europe, China and central to eastern USA. Large changes are also expected in the Sahel, but this region, like much of Brazil, India and southeast Asia, will see declines in overall burden. Hence, the change in pathogen assemblage in these areas is unlikely to pose a major threat to production. Europe, China and Peru are highlighted as regions where both overall burden and species turnover are greatest. These regions will therefore experience the greatest number of emerging, i.e. novel, pathogen pressure. Through the year, two pulses of pathogen assemblage change are seen at high latitude in the northern Hemisphere, first around April, second around September (Fig. 3). The largest changes in species composition are expected in October and November in northern USA and Canada, Europe, and northern China (Figs. 3, S13). The largest changes in the Sahel are seen during April and May, while the largest changes in India are seen during May and June.

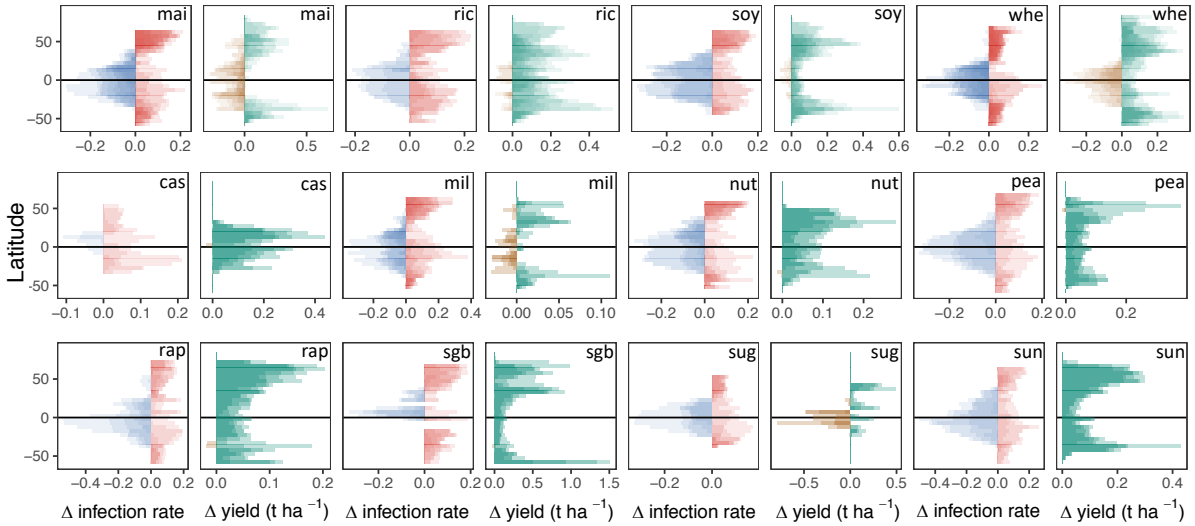

Fig 5. Changes in crop yield and pathogen infection rate under RCP 6.0. Major crops shown in the first row. (mai) maize, (ric) rice, (soy) soybean, (whe) wheat, (cas) cassava, (mil) millet, (nut) peanut, (pea) pea, (rap) rapeseed, (sgb) sugar beet, (sug) sugar cane, and (sun) sunflower. Red and blue indicate increases and decreases in pathogen infection rate, respectively. Green and brown indicate increases and decreases in crop yield, respectively. For major hosts, colour saturation for each crop model (LPJmL, GEPIC, PEPIC) climate model (GFDL-ESM2M, HADGEM2-ES, IPSL-CM5A-LR, MIROC5) combination was set to 1/12. For other hosts, colour saturation was set to 1/4 as only the LPJmL model was used. Colour saturation for each pathogen was set to 1/10 (min = 3, max = 15 pathogens per host, Table S2).

We validated our models against current known pathogen distributions (Fig. S9, Table S3). Temperature-related infection risk alone gave high false positive rates (predicting pathogen presence in regions where the pathogen is currently unreported). Restricting predicted distributions by host distributions improved overall model fit, reducing false positive rates and increasing true negative rates. High false positives rates were more likely in countries with low per capita GDP (Fig. S9), indicating an under-reporting bias in developing countries[5].

Model limitations

Our analyses are limited by the availability of infection temperature responses in the published literature. These are not a random sample of all known fungal and oomycete plant pathogens. Given that the historical research focus on plant pathogens has been in developed

191 countries at high latitudes [16], our sample is biased towards pathogens which have evolved to
192 infect hosts optimally in cooler climates (Fig. S14). However, our sample does include
193 pathogens able to infect both tropical and temperate crops (Figs. S7, S8), hence this bias does
194 not preclude conclusions being drawn for tropical pathogens.

195 We did not attempt to model intra-specific variation in temperature response functions, but
196 such variation does exist [17,18]. However, analysis of historical pathogen distributions indicates
197 that range shifts have occurred in line with expectation suggesting that temperature
198 adaptation is slow in comparison with climate change [7]. We employed infection temperatures
199 rather than the more commonly-measured growth in axenic culture [3], for all but two
200 pathogens which were included because of their importance in agriculture [1]. The distinction
201 is important because growth in culture has a wider temperature range for most pathogens [3],
202 and models based on growth in culture would suggest a wider geographical range than
203 models based upon infection dynamics.

204 We only considered temperature as a determinant of infection rates. Infection by many fungal
205 and oomycete plant pathogens is promoted by wet conditions [19]. Multi-model mean
206 projections for precipitation to the end of the 21st Century suggest that precipitation will
207 increase significantly in boreal regions and decrease significantly around the Mediterranean,
208 with smaller and less certain changes elsewhere even under a high-emissions scenario [20].
209 Thus, there appears to be no major change in hydrology that would alter our overall
210 conclusions on latitudinal shifts in pathogen burden. In addition, global observations[21] and
211 field-scale experiments[22] suggest that temperature is the most important determinant of
212 fungal distributions and activity.

213 We did not include potential future changes in crop phenology. Warming is expected to
214 extend the growing season of temperate crops by a few days by the end of the 21st Century,
215 while increasing temperatures may reduce the length of the growing season in tropical crops
216 [23]. As our seasonal modelling was conducted using monthly crop calendars, the influence of
217 altered growing seasons on our results is likely to be small. Finally, we did not include
218 potential future changes in crop distributions. The socioeconomic factors leading to changes
219 in future crop distributions are challenging to predict [24], and differing future land use
220 scenarios are beyond the scope of the present analysis.

Future crop yields have been modelled using only plant physiological responses to abiotic conditions. We analysed pathogen temperature physiology to understand how indirect, biotic responses to climate change could impact production. We have shown that crop disease burdens will track crop responses, increasing at higher latitudes where climate change is expected to boost yields. Furthermore, the suite of crop diseases that farmers face in some of the world's most productive regions will change dramatically. Agriculture must prepare accordingly if any potential benefits of climate change on crop yields are to be realized.

Acknowledgments

Funding: TMC is supported by a BBSRC SWBio DTP studentship BB/M009122/1. DB and SG are supported by BBSRC grant BB/N020847/1 and the Global Burden of Crop Loss project (Bill and Melinda Gates Foundation). SG is supported by a CIFAR Fellowship "The Fungal Kingdon: Threats and Opportunities".

Author contributions

DB and TC developed the concept, collated the data, conducted the analyses and prepared the figures. DB wrote the manuscript with contributions from TC and SG.

Methods

Crop yields

Annual crop yield projections from 2006-2099 were obtained from the Inter-Sectoral Model Intercomparison Project (ISIMIP, www.isimip.org). The crop models were LPJmL [11], GEPIC [25] and PEPIC [26]. GEPIC and PEPIC are derived from the EPIC agricultural yield and water quality model [27]. Each of these crop models was driven by four global circulation models: MIROC5 [28], HadGEM2-ES [29], GFDL-ESM2M [30] and IPSL-CM5A-LR [31]. Annual crop yield estimates under RCP 6.0, with CO_2 fertilization and no irrigation, were obtained for all available crops at 0.5 ° spatial resolution. GEPIC/PEPIC modelled maize, rice, soybean and wheat. LPJmL additionally included cassava, millet, pea, peanut, rapeseed, sugarbeet, sugarcane and sunflower. Yield differences between the 2060 – 2080 mean and 2010 – 2030 mean were calculated per grid cell.

Note on difference between modelled production and FAO reported production from 2006 to 2018 (Figs. S5, S15). For all crops except cassava and sugarcane, modelled total global

production was similar to reported production. For example, for maize the modelled production was 0.26 – 1.00 of reported production (per year and model), while for soybean it was 0.98 – 2.26 of reported production. Much of this deviation can be explained by increases in harvested area for most crops since 2000 (Fig. S15). For cassava, modelled production was 0.10 – 0.14 of reported production, and for sugarcane, 0.004 – 0.009 of reported production. These differences are caused by a mismatch between locations predicted as suitable for crop production by the LPJmL model, and the locations allocated to a crop in the Earthstat dataset. For the LPjML sugarcane model driven by HADGEM2, only 0.38 % of grid cells predicted to have yields above 30 t ha^{-1} (around half of current global mean yield) in 2006 were also predicted to contain a minimum of 1 % by area of sugarcane in 2000.

Climate data

Global estimates of current (1970 - 2000 average) and future (2061 - 2080 average) average monthly temperature at 5 arc minute spatial resolution were obtained from the WorldClim database (www.worldclim.org) [5/2019]. For future estimates, all global climate models (GCMs) of Representative Concentration Pathways (RCP) 2.6, 4.5, 6.0 and 8.5 were obtained (Table S4) [5/2019]. For each GCM, average future monthly temperature was calculated as the mid-point of average maximum and minimum monthly temperature, as no average estimates were available. For each RCP, average monthly temperature was calculated as the median of all GCMs for that RCP.

Pathogen dataset construction

Estimates of pathogen infection cardinal temperature were extracted from two sources [3,32]. Collectively, only pathogens with at least one minimum (T_{min}), optimum (T_{opt}), and maximum (T_{max}) estimate for infection cardinal temperature were included. To aid matching of species between sources, pathogen species names reported in the latter were updated according to the Species Fungorum database (SFD) (www.speciesfungorum.org) [accessed April, 2020] (Table S5). If no information was available on the SFD, Mycobank (www.mycobank.org) was used as an alternative [accessed April, 2020]. Discovery and sanction author(s) of species were not provided in one source [32], and are not considered here. Pathogen species names have previously been processed [3] and so were not processed further. Mean T_{min}, T_{opt}, and T_{max} infection cardinal temperature were calculated for each pathogen (hereafter referred to as the 'Pathogen dataset'). *Magnaporthe oryzae* and *Zymoseptoria*

tritici are two of the most destructive pathogens of rice and wheat [1], respectively, but infection temperature estimates are unavailable. We therefore included cardinal temperature for lesion development of *M. oryzae* [33], and average growth in culture cardinal temperatures for 18 strains of *Z. tritici* [34]. It was assumed that average cardinal temperature for each pathogen was identical across all hosts, for each respective pathogen.

The Plantwise database (CABI) [accessed 28/10/2013, by permission] was used to estimate host range of each pathogen in the Pathogen dataset. To improve matching of pathogen species names, some names were updated in the Plantwise database, according to the SFD or Mycobank [accessed 2019 - 2020] (Table S1). All plant-pathogen interaction records for hosts recorded in EarthStat (http://www.earthstat.org) and MIRCA2000 [35] were extracted from the Plantwise database. To improve matching of host species, scientific names were assigned to plant hosts found in EarthStat and MIRCA2000 (Table S6). Pathogens absent from the extracted plant-pathogen interaction dataset were excluded from the Pathogen dataset. Consequently, 79 pathogens were included in the Pathogen dataset and hence included in this study (Fig. 1, Table S1).

Estimating global distributions of pathogen hosts

Two approaches were used to estimate global host distributions for each pathogen included in the Pathogen dataset. First, for 145 crops (including forage crops, Table S6), global estimates of average fractional proportion grid cell harvested (5 arc minute spatial resolution) were obtained from EarthStat (http://www.earthstat.org). Only crops that could be clearly identified in the Plantwise database were included (i.e. “mixed grain” was not included). Each crop map was converted to binary presence/absence. If grid cell harvest area fraction was ≥ 0.00001 (equivalent to 0.1 m^2 ha^{-1}), the host was estimated as present in said grid cell. If < 0.00001, hosts were assumed absent. These values were chosen to ensure that crops were estimated as present in grid cells, even if average fractional proportion harvested were estimated as very small. This approach enabled estimation of global distribution for each crop in EarthStat.

Second, for 24 crops (Table S6), global estimates of growing season periods (around the year 2000) were extracted from MIRCA2000 at 30 arc minute spatial resolution, and resampled to 5 arc minute resolution using neighbour joining algorithm in package *raster* for R [36]. For each crop, rainfed and irrigated growing season estimates were combined. This provided

312 global monthly estimates of global host presence (within growing season) and absence
313 (outside of growing season), and hence monthly global distribution estimates, at 5 arc minute
314 spatial resolution for 24 crops.

315 For each pathogen, global distributions for all recorded hosts were combined, and converted
316 to binary presence/absence. This provided a single potential geographical distribution of each
317 pathogen, based on reported pathogen host range (Plantwise) and geographic host
318 distributions (EarthStat or MIRCA2000) (Fig. S7, S8). For example, if a pathogen was
319 recorded in the Plantwise database to successfully infect four hosts recorded in EarthStat, any
320 grid cells that were estimated to contain ≥1 of these hosts (as above) were converted to 1
321 (present), and grid cells that there were estimated to contain 0 hosts were converted to 0
322 (absent). This was done independently for host distributions estimated from EarthStat and
323 MIRCA2000, resulting in two alternative potential geographical distribution of each
324 pathogen. Where MIRCA2000 was utilised, fewer pathogens were included, due to fewer
325 included crop species. Further, where host range was estimated from MIRCA2000, the
326 potential geographical range of a pathogen of estimated each month, due to host growing
327 season (Fig. S8). Host ranges were assumed independent for each pathogen, i.e. competition
328 between pathogens for particular hosts was assumed to not occur.

329 *Modelling pathogen temperature suitability*

330 In all analyses, for each pathogen, average monthly temperature (T) suitable for host
331 infection was assumed to be any temperature within $T_{min(0.5)}$ and $T_{max(0.5)}$ of the pathogens
332 cardinal temperature, referred to as $T_{range(0.5)}$. $T_{min(0.5)}$ and $T_{max(0.5)}$ refer to temperatures where
333 a pathogens infection response rate = 0.5 (at T_{opt} the responses = 1, at T_{min} and T_{max} the
334 response = 0) (Fig. 1, Table S1). Pathogen temperature responses were calculated by a beta
335 function [37] (Equation S1). If average monthly (i) grid cell (j) temperature ($T_{\{i,j\}}$) fell within a
336 pathogens $T_{range(0.5)}$, the grid cell was deemed suitable for host infection, and hence the
337 pathogen was recorded as 'present'. Pathogens were recorded as 'absent' for all other grid
338 cells.

339 $$\text{Equation S1: } r\left(T_{\{i,j\}}\right) = \left(\frac{T_{max} - T_{\{i,j\}}}{T_{max} - T_{opt}}\right)\left(\frac{T_{\{i,j\}} - T_{min}}{T_{opt} - T_{min}}\right)^{(T_{opt}-T_{min})/(T_{max}-T_{opt})}$$

340 *Model validation*

Pathogen presence was calculated for current average monthly temperature estimates utilising two alternative approaches. In the 'climate-only model', pathogens were not restricted by host distributions. In the 'climate-host model', pathogens were additionally restricted by host distributions estimated from EarthStat. In both model iterations, a summary global distribution of each pathogen was calculated, whereby if a pathogen was modelled as present in a grid cell (j) during any month (i), then the pathogen was classed as 'present' in that grid cell (j). Outputs from both model iterations were then compared to observed records of pathogen presence at country or state scale (hereafter collectively referred to as 'region', 396 regions total), from the CABI Plantwise database. Pathogen names in this dataset were updated according to the SFD or Mycobank [accessed 2019 - 2020] to improve matching to the Pathogen dataset (Table S7). Discovery and sanction author(s) of species were not provided in this dataset, and so were not considered here. 13 pathogens (*Alternaria cucumerina*, *Botrytis cinerea*, *Cercospora carotae*, *Didymella arachidicola*, *Diplocarpon earlianum*, *Fusarium oxysporum f.sp. conglutinans*, *Fusarium roseum*, *Globisporangium ultimum*, *Nothopassalora personata*, *Puccinia menthae*, *Septoria glycines*, *Stigmina carpophila*, and *Wilsoniana occidentalis*) were excluded from model validation, due to an apparent lack of observational records.

Models were run at 5 arc minute resolution, whereas observed pathogen records were at regional scale (Fig. S9a, c). Hence, model outputs were summed to regional scale (Fig. S9b, d). If a pathogen was modelled as 'present' in any grid cell (j) in a region, for any month (i), the pathogen was modelled as 'present' at the regional scale. Country-level gross domestic product based on purchasing power parity (GDP (PPP)) and research output (number of publications) were obtained from the World Bank Data website (data.worldbank.org) [accessed November 2018]. For the climate-host model, GDP (PPP) and research output were compared by Welch's Two Sample t-test between countries where (1) both the climate-host model estimated, and the CABI Distribution Maps of Plant Diseases recorded, a pathogen as present (true positive (Sensitivity)), and where (2) the climate-host model estimated a pathogen as present, but the CABI Distribution Maps of Plant Diseases recorded a pathogen as absent (false positive (Type 1 error)). Where GDP (PPP) and research output were recorded at country scale, but pathogen records were recorded are state scale, states were assigned country-level GDP (PPP) and research output.

Changes in global pathogen infection temperature suitability

Pathogen presence was calculated for current and future average monthly (i) grid cell (j) temperature ($T_{\{i,j\}}$), utilising two alternative host-restriction approaches. First, pathogens were restricted by host distributions estimated from EarthStat, for each future climate scenarios (RCP 2.6, 4.5, 6.0, and 8.5). Second, pathogens were restricted by host distributions estimated from MIRCA2000, and RCP 6.0 was used to estimate future average monthly temperature. This allowed for comparison between host restriction method on model outputs of change in spatial patterns of pathogen infection temperature suitability.

For each model, the change in pathogen burden was calculated as the difference in pathogens modelled as 'present' under future climate conditions, minus those under current climate, for each grid cell (j), for each month (i). Within a grid cell, increases or decreases in pathogen burden do not reflect the change of species composition [8]. Therefore, for each model, a modified Jaccard (J) index (1 - J) of community dissimilarity (species turnover) [8,38] was calculated to characterize the change in community composition in each grid cell (j), for each month (i). High pathogen turnover represents high community dissimilarity or high species turnover, indicating a high change in species composition.

Change in pathogen infection rate under RCP 6.0

Change in spatial patterns of pathogen infection temperature suitability was calculated, as above, with the following modifications. First, a model was constructed for each host separately, using MIRCA2000 estimates of host distributions. Second, pathogen infection rate was not converted to binary presence/absence using $T_{range(0.5)}$. Instead, the change in a pathogens infection rate was calculated as the difference in infection rate under future climate conditions, minus that calculated under current climate, for each pathogen, for each grid cell (j), for each month (i). Only RCP 6.0 was used for future estimates of global temperature. We used estimates from MIRCA2000 for pulses as a proxy for pea crop (*Pisum sativum*). The average change of infection rate for each pathogen was calculated at each latitude (5 arc minute resolution), and then averaged to 5-degree resolution. The calculated average change in pathogen infection rate was compared to climate change-driven changes in yield for each crop, respectively. The number of pathogens included for each host is provided in Table S2.

Pathogen sampling bias

Northern and southern latitudinal ranges for plant pests and pathogens were extracted from the CABI Plantwise database. As above, some pathogen names in this dataset were updated

404 according to the SFD or Mycobank [accessed 2019 – 2020] to improve matching to the
405 Pathogen dataset (Table S7) and 13 pathogens were excluded from the analysis, due to an
406 apparent lack of observational records. Pathogen names were not updated in this dataset if
407 they were absent from the Pathogen dataset. Northern and southern latitudinal ranges for
408 pathogens included in the Pathogen dataset were compared to that of all fungi and oomycetes
409 pathogens for which latitudinal ranges were available.

410 **References**

411 1. Fones, H. N. *et al.* Threats to global food security from emerging fungal and oomycete
412 crop pathogens. *Nature Food* **In press**, (2020).
413 2. Savary, S. *et al.* The global burden of pathogens and pests on major food crops. *Nature*
414 *Ecology & Evolution* **3**, 430–439 (2019).
415 3. Chaloner, T. M., Gurr, S. J. & Bebber, D. P. Geometry and evolution of the ecological
416 niche in plant-associated microbes. *bioRxiv* 836411 (2019) doi:10.1101/836411.
417 4. Bebber, D. P. Range-Expanding Pests and Pathogens in a Warming World. *Annu. Rev.*
418 *Phytopathol.* **53**, 335–356 (2015).
419 5. Bebber, D. P. *et al.* Many unreported crop pests and pathogens are probably already
420 present. *Global Change Biology* **25**, 2703–2713 (2019).
421 6. Parmesan, C. Ecological and evolutionary responses to recent climate change. *Annual*
422 *Review of Ecology & Systematics* **37**, 637–669 (2006).
423 7. Bebber, D. P., Ramotowski, M. A. T. & Gurr, S. J. Crop pests and pathogens move
424 polewards in a warming world. *Nature Clim. Change* **3**, 985–988 (2013).
425 8. Yan, Y., Wang, Y.-C., Feng, C.-C., Wan, P.-H. M. & Chang, K. T.-T. Potential
426 distributional changes of invasive crop pest species associated with global climate
427 change. *Applied Geography* **82**, 83–92 (2017).

9. Elith, J. & Leathwick, J. R. Species Distribution Models: Ecological Explanation and Prediction Across Space and Time. *Annual Review of Ecology, Evolution, and Systematics* **40**, 677–697 (2009).
10. Kearney, M. & Porter, W. Mechanistic niche modelling: combining physiological and spatial data to predict species' ranges. *Ecology Letters* **12**, 334–350 (2009).
11. Bondeau, A. *et al.* Modelling the role of agriculture for the 20th century global terrestrial carbon balance. *Global Change Biology* **13**, 679–706 (2007).
12. Bregaglio, S., Donatelli, M. & Confalonieri, R. Fungal infections of rice, wheat, and grape in Europe in 2030–2050. *Agron. Sustain. Dev.* **33**, 767–776 (2013).
13. Bebber, D. P. Climate change effects on Black Sigatoka disease of banana. *Philosophical Transactions of the Royal Society B: Biological Sciences* **374**, 20180269 (2019).
14. Rosenzweig, C. *et al.* Assessing agricultural risks of climate change in the 21st century in a global gridded crop model intercomparison. *PNAS* **111**, 3268–3273 (2014).
15. Bebber, D. P., Holmes, T. & Gurr, S. J. The global spread of crop pests and pathogens. *Glob. Ecol. Biogeogr.* **23**, 1398–1407 (2014).
16. Bebber, D. P., Holmes, T., Smith, D. & Gurr, S. J. Economic and physical determinants of the global distributions of crop pests and pathogens. *New Phytol.* **202**, 901–910 (2014).
17. Zhan, J. & McDonald, B. A. Thermal adaptation in the fungal pathogen Mycosphaerella graminicola. *Molecular Ecology* **20**, 1689–1701 (2011).
18. Robin, C., Andanson, A., Saint-Jean, G., Fabreguettes, O. & Dutech, C. What was old is new again: thermal adaptation within clonal lineages during range expansion in a fungal pathogen. *Molecular Ecology* **26**, 1952–1963 (2017).
19. Rowlandson, T. *et al.* Reconsidering Leaf Wetness Duration Determination for Plant Disease Management. *Plant Disease* **99**, 310–319 (2014).

20. IPCC. *Climate Change 2013: The Physical Science Basis. Contribution of Working Group I to the Fifth Assessment Report of the Intergovernmental Panel on Climate Change*. (Cambridge University Press, 2013).
21. Větrovský, T. *et al.* A meta-analysis of global fungal distribution reveals climate-driven patterns. *Nature Communications* **10**, 1–9 (2019).
22. Liu, X. *et al.* Warming affects foliar fungal diseases more than precipitation in a Tibetan alpine meadow. *New Phytologist* **221**, 1574–1584 (2019).
23. IPCC. *Climate Change 2014: Impacts, Adaptation, and Vulnerability. Part A: Global and Sectoral Aspects. Contribution of Working Group II to the Fifth Assessment Report of the Intergovernmental Panel on Climate Change*. (Cambridge University Press, 2014).
24. Sohl, T. L., Wimberly, M. C., Radeloff, V. C., Theobald, D. M. & Sleeter, B. M. Divergent projections of future land use in the United States arising from different models and scenarios. *Ecological Modelling* **337**, 281–297 (2016).
25. Liu, J., Williams, J. R., Zehnder, A. J. B. & Yang, H. GEPIC – modelling wheat yield and crop water productivity with high resolution on a global scale. *Agricultural Systems* **94**, 478–493 (2007).
26. Liu, W. *et al.* Global investigation of impacts of PET methods on simulating crop-water relations for maize. *Agricultural and Forest Meteorology* **221**, 164–175 (2016).
27. Williams, J. R. & Sharpley, A. N. *EPIC - Erosion/Productivity Impact Calculator: 1. Model documentation*. (1989).
28. Watanabe, M. *et al.* Improved Climate Simulation by MIROC5: Mean States, Variability, and Climate Sensitivity. *J. Climate* **23**, 6312–6335 (2010).
29. Collins, W. J. *et al.* Development and evaluation of an Earth-System model – HadGEM2. *Geoscientific Model Development* **4**, 1051–1075 (2011).

476 30. Dunne, J. P. *et al.* GFDL's ESM2 Global Coupled Climate–Carbon Earth System
477 Models. Part I: Physical Formulation and Baseline Simulation Characteristics. *J. Climate*
478 **25**, 6646–6665 (2012).
479 31. Dufresne, J.-L. *et al.* Climate change projections using the IPSL-CM5 Earth System
480 Model: from CMIP3 to CMIP5. *Clim Dyn* **40**, 2123–2165 (2013).
481 32. Magarey, R. D., Sutton, T. B. & Thayer, C. L. A Simple Generic Infection Model for
482 Foliar Fungal Plant Pathogens. *Phytopathology*^{TM} **95**, 92–100 (2005).
483 33. Viswanath, K. *et al.* Simulation of leaf blast infection in tropical rice agro-ecology under
484 climate change scenario. *Climatic Change* **142**, 155–167 (2017).
485 34. Boixel, A.-L., Delestre, G., Legeay, J., Chelle, M. & Suffert, F. Phenotyping Thermal
486 Responses of Yeasts and Yeast-like Microorganisms at the Individual and Population
487 Levels: Proof-of-Concept, Development and Application of an Experimental Framework
488 to a Plant Pathogen. *Microb Ecol* **78**, 42–56 (2019).
489 35. Portmann, F. T., Siebert, S. & Döll, P. MIRCA2000—Global monthly irrigated and
490 rainfed crop areas around the year 2000: A new high-resolution data set for agricultural
491 and hydrological modeling. *Global Biogeochemical Cycles* **24**, 1–24 (2010).
492 36. Hijmans, R. J. *et al. raster: Geographic Data Analysis and Modeling*. (2020).
493 37. Yan, W. & Hunt, L. A. An Equation for Modelling the Temperature Response of Plants
494 using only the Cardinal Temperatures. *Ann Bot* **84**, 607–614 (1999).
495 38. Wiens, J. A., Stralberg, D., Jongsomjit, D., Howell, C. A. & Snyder, M. A. Niches,
496 models, and climate change: Assessing the assumptions and uncertainties. *PNAS* **106**,
497 19729–19736 (2009).
498